

Signatures of Majorana Zero Modes in Spin-Resolved Current Correlations

Arbel Haim,¹ Erez Berg,¹ Felix von Oppen,² and Yuval Oreg¹

¹*Department of Condensed Matter Physics, Weizmann Institute of Science, Rehovot 76100, Israel*

²*Dahlem Center for Complex Quantum Systems and Fachbereich Physik, Freie Universität Berlin, 14195 Berlin, Germany*

(Received 11 November 2014; published 24 April 2015)

We consider a normal lead coupled to a Majorana bound state. We show that the spin-resolved current correlations exhibit unique features which distinguish Majorana bound states from other low-energy resonances. In particular, the spin-up and spin-down currents from a Majorana bound state are anticorrelated at low bias voltages, and become uncorrelated at higher voltages. This behavior is independent of the exact form of coupling to the lead, and of the direction of the spin polarization. In contrast, an ordinary low-energy Andreev bound state gives rise to a positive correlation between the spin-up and spin-down currents, and this spin-resolved current-current correlation approaches a nonzero constant at high bias voltages. We discuss experimental setups in which this effect can be measured.

DOI: 10.1103/PhysRevLett.114.166406

PACS numbers: 71.10.Pm, 72.25.-b, 74.45.+c, 74.78.Na

Introduction.—Majorana fermions in condensed matter systems [1,2] are zero-energy excitations which behave as particles which are their own antiparticles. The interest in phases which host such Majorana bound states (MBSs) stems largely from their topological nature; such a state stores information nonlocally. A consequence of this property is that such systems are insensitive to local perturbations and to decoherence [3]. This, along with their non-Abelian exchange statistics [4–7], makes them a potential platform for fault-tolerant quantum information processing [8].

In recent years various mechanisms have been proposed theoretically for realizing MBSs [4,9–16]. Specifically, it was predicted that a semiconductor nanowire with strong spin-orbit coupling in proximity to an s -wave superconductor and subject to a magnetic field can host localized MBSs [15,16]. This proposal prompted a series of transport experiments [17–21] reporting the observation of a zero-bias conductance peak (ZBCP), consistent with the presence of a MBS [22–24]. Very recently zero-energy states have also been detected at the ends of a ferromagnetic atomic chain deposited on a superconductor [25]. While these experiments are promising, it has been suggested that the ZBCP can also appear in the absence of a MBS as a result of other mechanisms [26–31]. It is therefore crucial to have a physical signature beyond the ZBCP, which will be able to distinguish the MBS from other possible physical scenarios.

In this Letter, we discuss the signatures of MBSs in spin-resolved current correlations. Consider a normal metallic lead coupled to a topological superconductor with a MBS at its end. A bias voltage is applied between the lead and the superconductor, driving a current from the lead. We are interested in the spin-resolved current correlations in the lead, defined as

$$P_{ss'} = \int_{-\infty}^{\infty} dt \langle \delta \hat{I}_s(0) \delta \hat{I}_{s'}(t) \rangle, \quad \delta \hat{I}_s = \hat{I}_s - \langle \hat{I}_s \rangle, \quad (1)$$

where \hat{I}_s is the spin- s current operator ($s = \uparrow, \downarrow$). We concentrate on the cross correlation term $P_{\uparrow\downarrow}$ and compare between two cases: with a MBS present, and with an “accidental” low-energy Andreev bound state (ABS) but without a MBS. Both cases lead to a similar ZBCP.

As we will show, in the presence of a MBS, the cross term $P_{\uparrow\downarrow}$ carries unique signatures, that are strikingly different from the case of an ABS: In the MBS case, $P_{\uparrow\downarrow}$ is negative in sign, and approaches zero as $P_{\uparrow\downarrow} \propto 1/V$ with increasing bias voltage V . In contrast, an ABS generically gives rise to a positive $P_{\uparrow\downarrow}$, that approaches a nonzero constant at high voltages. Notice that a low-energy ABS can be viewed as a pair of overlapping MBSs. Crucially, however, unlike the case of two spatially separated MBSs, in this case both MBSs are coupled to the lead with comparable strengths.

As a prototypical setup for measuring this effect, we consider a long semiconductor nanowire proximity coupled to a conventional bulk s -wave superconductor (Fig. 1). Under the right conditions, a MBS is formed at the end of the wire [15,16]. The wire is tunnel coupled to a normal lead forming a T junction; a bias voltage is applied between the lead and the superconductor. At the two arms of the T junction, there are “spin filters” that allow only electrons of a certain spin polarization to pass. Physical ways to implement such spin filters will be discussed below. This setup allows measurement of the correlation functions defined in Eq. (1), including $P_{\uparrow\downarrow}$ for oppositely polarized spin filters.

Intuitive analysis.—The behavior of $P_{\uparrow\downarrow}$ can be understood from qualitative considerations. We assume that the bias voltage is smaller than the gap of the superconductor, such that only Andreev reflection [32] in the lead contributes to the conductance. Consider first the case $V \gg \Gamma$, where Γ is the width of the ZBCP (originating either from a MBS or an accidental low-energy ABS near the end of the

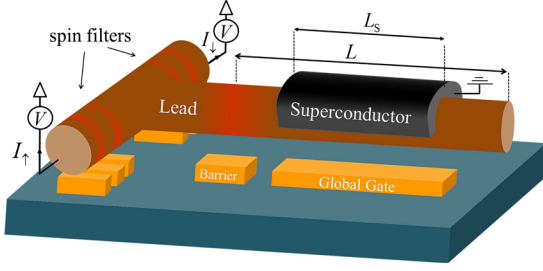


FIG. 1 (color online). A semiconductor nanowire proximity coupled to an s -wave superconductor. Under certain conditions the system hosts Majorana bound states at its ends. The system is tunnel coupled on the left to a normal lead which is biased at a voltage V . The correlations between the spin-resolved currents (I_{\uparrow} and I_{\downarrow}) in the normal lead have features which are unique to the Majorana bound state. To measure these correlations we suggest implementing the system in a T -shaped junction and placing a “spin filter” at each of the arms of the T . This may be done by defining quantum dots using gate voltages. In the presence of a magnetic field the resonance level of each dot can be tuned by back gates to have opposite spins.

wire). In this limit one can discuss sequential single-particle tunneling events. As Cooper pairs are transported from the superconductor to the lead, they split such that one electron goes to the lead while the other electron changes the occupation of the low-energy resonance [33].

A change in the occupation number of an ordinary ABS is generically accompanied by a change in local physical observables near the edge, e.g., the local spin and charge densities. As a result, the spin density near the edge changes each time an electron is transmitted and the spin of the transmitted electron tends to be antialigned with the spin of the preceding transmitted electron. (If the z component of the spin is conserved, this correlation is perfect.) Such a correlation corresponds to $P_{\uparrow\downarrow} > 0$.

On the other hand, a change in the occupation number of a MBS cannot be detected in *any* local observable near a single edge. In particular, the local spin densities of the two degenerate ground states (associated with the occupation number of the fermion formed by the MBSs at the two ends) are identical [34]. It follows that the spins of consecutive electrons are uncorrelated; hence $P_{\uparrow\downarrow} \rightarrow 0$.

Next, consider the case $V, T \ll \Gamma$ (where T is the temperature). In the MBS case, the total shot-noise power $P = \sum_{s,s'=\uparrow,\downarrow} P_{ss'}$ goes to zero as a result of the total transmission approaching unity [22–24]. Since $P_{\uparrow\uparrow}$ and $P_{\downarrow\downarrow}$ are positive definite quantities, we must have $P_{\uparrow\downarrow} = P_{\downarrow\uparrow} \leq 0$.

Simple model.—With this qualitative picture in mind, we calculate $P_{ss'}$ for a general low-energy model $H = H_L + H_T$ of a normal lead coupled to a MBS, where

$$H_L = \sum_{k,s} \epsilon_k \psi_{ks}^\dagger \psi_{ks}, \quad H_T = i\gamma \sum_{k,s} (t_s \psi_{ks} + \text{H.c.}). \quad (2)$$

Here ψ_{ks} describes the lead modes with spin s , ϵ_k are the energy levels in the lead, and t_s is the coupling constant of these modes to the Majorana state described by γ [35]. The form of H is quite general and stems solely from the Hermitian nature of γ .

At energies below the superconducting gap only reflection processes are possible, and the scattering matrix is given by [36,37]

$$\begin{pmatrix} r^{ee} & r^{eh} \\ r^{he} & r^{hh} \end{pmatrix} = 1 - 2\pi i W^\dagger (E + i\pi W W^\dagger)^{-1} W, \quad (3)$$

with $W = \sqrt{\nu_0}(t_\uparrow, t_\downarrow, t_\uparrow^*, t_\downarrow^*)$, and where ν_0 is the density of states in the lead. This yields

$$r_{ss'}^{ee} = \delta_{ss'} + \frac{2\pi\nu_0 t_s^* t_{s'}}{iE - \Gamma}, \quad r_{ss'}^{he} = \frac{2\pi\nu_0 t_s t_{s'}}{iE - \Gamma} \quad (4)$$

where $r^{hh}(E) = [r^{ee}(-E)]^*$, $r^{eh}(E) = [r^{he}(-E)]^*$ as dictated by particle-hole symmetry, and $\Gamma = 2\pi\nu_0(|t_\uparrow|^2 + |t_\downarrow|^2)$.

The spin-resolved currents and their correlation functions are given by [38]

$$\begin{aligned} \langle \hat{I}_s \rangle &= \frac{e}{h} \sum_{s' \in \uparrow, \downarrow} \text{sgn}(\alpha) \int_0^\infty dE A_{s's'}^{\beta\beta}(s, \alpha; E) f_\beta(E), \\ P_{ss'} &= \frac{e^2}{h} \sum_{\sigma, \sigma' \in \uparrow, \downarrow} \text{sgn}(\alpha) \text{sgn}(\beta) \int_0^\infty dE \\ &\quad \times A_{\sigma\sigma'}^{\gamma\delta}(s, \alpha; E) A_{\sigma\sigma'}^{\delta\gamma}(s', \beta; E) f_\gamma(E) [1 - f_\delta(E)], \\ A_{\sigma\sigma'}^{\gamma\delta}(s, \alpha; E) &= \delta_{s\sigma} \delta_{s'\sigma'} \delta_{\alpha\gamma} \delta_{\beta\delta} - [r_{s\sigma}^{\alpha\gamma}]^* r_{s'\sigma'}^{\beta\delta}, \end{aligned} \quad (5)$$

with $f_e(E) = 1 - f_h(-E)$ being the distribution of incoming electrons in the lead. Here $\text{sgn}(\alpha) = +1$ for $\alpha = e$ and $\text{sgn}(\alpha) = -1$ for $\alpha = h$. Inserting the reflection matrices of Eq. (4), one obtains at zero temperature

$$P_{\uparrow\downarrow} = -\frac{2e^2}{h} \Gamma_\uparrow \Gamma_\downarrow \frac{eV}{(eV)^2 + \Gamma^2}, \quad (6)$$

where $\Gamma_s = 2\pi\nu_0 |t_s|^2$. As anticipated, $P_{\uparrow\downarrow}$ is negative and goes to zero at high voltages as $1/V$ (assuming eV remains smaller than the superconducting gap). We note that summing $P_{\uparrow\downarrow}$ with the rest of the spin-resolved terms gives the total shot noise power [23,39–41].

The result of Eq. (6) does not depend on details such as the particular system hosting the MBS, the nature of the coupling to the lead, or the particular spin polarization axis. One can change the spin axis by transforming the coupling constants according to

$$\begin{pmatrix} t'_\uparrow & t'_\downarrow \end{pmatrix} = \begin{pmatrix} t_\uparrow & t_\downarrow \end{pmatrix} \exp(-i\theta \hat{\mathbf{n}} \cdot \boldsymbol{\sigma}/2), \quad (7)$$

where $\boldsymbol{\sigma}$ is a vector of Pauli matrices, $\hat{\mathbf{n}}$ is a unit vector and θ is a rotation angle. We note in passing that by varying both $\hat{\mathbf{n}}$ and θ one can always find a spin axis such that $t'_\downarrow = 0$ [42], resulting in a spin-polarized current [43].

Next, we consider an accidental low-energy ABS. For simplicity we shall temporarily assume that spin in the z direction is conserved [44]. Under these assumptions the most general tunneling Hamiltonian is given by [45]

$$\tilde{H}_T = a^\dagger \sum_k (\tilde{t}_\uparrow \psi_{k\uparrow} + \tilde{t}_\downarrow \psi_{k\downarrow}^\dagger) + \text{H.c.}, \quad (8)$$

where a is the annihilation operator for the ABS. (Notice that if one writes a in terms of two Majorana operators, then both of them are coupled to the lead with equal strength.) One can now use Eq. (3) with

$$W = \sqrt{\nu_0} \begin{pmatrix} \tilde{t}_\uparrow & 0 & 0 & \tilde{t}_\downarrow^* \\ 0 & \tilde{t}_\downarrow & \tilde{t}_\uparrow^* & 0 \end{pmatrix}, \quad (9)$$

to obtain the reflection matrices

$$r^{ee} = \frac{iE}{iE - \tilde{\Gamma}/2} + \frac{(\tilde{\Gamma}_\uparrow - \tilde{\Gamma}_\downarrow)/2}{iE - \tilde{\Gamma}/2} \sigma^z, \quad r^{he} = \frac{2\pi\nu_0 \tilde{t}_\uparrow \tilde{t}_\downarrow}{iE - \tilde{\Gamma}/2} \sigma^x. \quad (10)$$

These reflection matrices are written in the basis of the spin in the z direction. To obtain them for a general spin direction, we perform a transformation on r^{ee} , r^{he} which rotates the spin axis by an angle θ away from the z axis [45]. Upon doing so, and then using Eq. (5) one has

$$P_{\uparrow\downarrow} = \frac{2e^2}{h} \frac{\tilde{\Gamma}_\uparrow \tilde{\Gamma}_\downarrow}{\tilde{\Gamma}} \left\{ \left[\frac{(\tilde{\Gamma}_\uparrow - \tilde{\Gamma}_\downarrow)^2}{\tilde{\Gamma}^2} + \cos^2 \theta \right] \arctan \frac{2eV}{\tilde{\Gamma}} + \left[\frac{(\tilde{\Gamma}_\uparrow - \tilde{\Gamma}_\downarrow)^2}{\tilde{\Gamma}^2} - \cos^2 \theta \right] \frac{2eV/\tilde{\Gamma}}{1 + (2eV/\tilde{\Gamma})^2} \right\}. \quad (11)$$

This should be compared to Eq. (6). Unlike the MBS scenario, $P_{\uparrow\downarrow}$ is now positive for all V and monotonically approaches a finite value at $eV \gg \tilde{\Gamma}$.

Microscopic model.—Next we verify our conclusions using a numerical simulation of an experimentally realizable microscopic model [17–20]. We consider a nanowire having Rashba spin-orbit coupling, proximity coupled to an s -wave superconductor, with an applied Zeeman field. The wire is tunnel coupled to a normal lead from the left, as depicted in Fig. 1. The Hamiltonian for the system (not including the spin filters) is $H = H_L + H_{\text{nw}} + H_T$, with H_L being the isolated lead Hamiltonian in Eq. (2), H_{nw} is the Hamiltonian for the nanowire given by

$$H_{\text{nw}} = \int_{-L/2}^{L/2} dx \Phi^\dagger(x) \mathcal{H} \Phi(x),$$

$$\mathcal{H} = \left(\frac{-\partial_x^2}{2m_e} - \mu \right) \tau^z + i\alpha_R \tau^z \sigma^z \partial_x + \mathbf{B} \cdot \boldsymbol{\sigma} + \Delta(x) \tau^x, \quad (12)$$

where $\Phi^\dagger(x) = (\phi_\uparrow^\dagger(x), \phi_\downarrow^\dagger(x), \phi_\downarrow(x), -\phi_\uparrow(x))$ are the electron creation and annihilation operators in the wire, and H_T describes the coupling of the nanowire to the lead

$$H_T = - \sum_{k,p,s} t_{kp} \phi_{ps}^\dagger \psi_{ks} + \text{H.c.} \quad (13)$$

Here ϕ_{ps} denotes an eigenmode of the decoupled wire, t_{kp} are the hopping matrix elements between the lead and the wire, m_e is the effective electron mass, μ is the chemical potential, α_R describes the spin-orbit coupling, \mathbf{B} is the Zeeman field, and $\Delta(x) = \Delta_0 \theta(L_S/2 - |x|)$ is the induced pair potential in the wire, with L_S being the length of the section of the wire which is covered by the superconductor (cf. Fig. 1).

As we shall now show, this system can exhibit either a zero-energy ABS or a zero-energy MBS at the end of the wire, depending on the value of B . The differential conductance spectra in the two cases are similar. The spin-resolved current correlations, however, are qualitatively different. By discretizing H on a lattice we numerically obtain the scattering matrix [45], from which the spin-resolved currents and their correlations are obtained with the help of Eq. (5).

In Fig. 2(a) the differential conductance $d\langle \hat{I} \rangle / dV$ is presented as a function of bias voltage V and Zeeman energy B , for a value of $\mu = 125 \mu\text{eV}$ and at a temperature of $T = 30 \text{ mK}$. The magnetic field \mathbf{B} is applied at an angle of 60° from the z axis in the xz plane. The dashed white line signifies the critical Zeeman energy $B_c = \sqrt{\mu^2 + \Delta_0^2}$ above which the system is in the topological phase in the thermodynamic limit [15,16]. Beyond this a zero-energy MBS appears, and one observes a ZBCP. At even higher magnetic fields the conductance begins to oscillate due to the overlap between the MBSs at the two ends of the wire [19,46–48].

Importantly, a ZBCP is also present at a magnetic field which is *below* the critical line, at about $B \sim 0.1 \text{ meV}$, even though the system is in the topologically trivial phase. This ZBCP is due to a trivial ABS which is localized at the left end of the wire. In Fig. 2(b) the local density of states (LDOS) at zero energy $\mathcal{N}(x, 0)$ [45] is presented for two different Zeeman energies $B = 350 \mu\text{eV}$ and $B = 90 \mu\text{eV}$, corresponding to the MBS and ABS, respectively. We note that in both cases the LDOS is peaked at the two ends of the wire [49], making it difficult to distinguish between the ABS and the MBS via a scanning tunneling microscopy measurement.

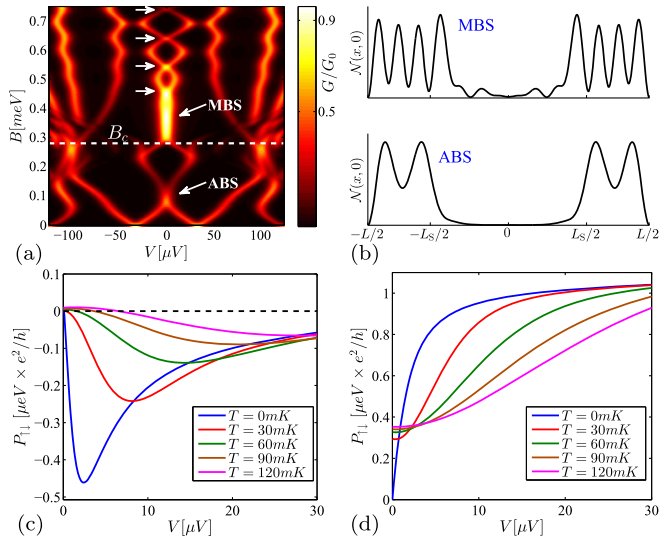


FIG. 2 (color online). Numerical simulation of the system described in Eq. (12) and depicted in Fig. 1. The parameters of the system are taken to be in accordance with a recent experiment [17], namely, $E_{\text{so}} = m_e \alpha_R^2 / 2 = 50 \mu\text{eV}$, $\Delta_0 = 250 \mu\text{eV}$, and $l_{\text{so}} = 1 / (m_e \alpha_R) = 200 \text{ nm}$. We take the length of the wire to be $L = 2.5 \mu\text{m}$ with $L_S = 1.4 \mu\text{m}$. Similar results are obtained for parameters taken from a different experiment [19,45]. The magnetic field \mathbf{B} is applied at an angle of 60° from the z axis in the xz plane. (a) Differential conductance as a function of bias V and Zeeman energy B for $\mu = 125 \mu\text{eV}$ and at $T = 30 \text{ mK}$, in units of $G_0 = e^2/h$. A zero-bias conductance peak appears both as a result of a Majorana bound state (MBS) at $B > B_c$, and as a result of a trivial Andreev bound state (ABS) at $B < B_c$. (b) Local density of state at zero energy for $B = 350 \mu\text{eV}$ and for $B = 90 \mu\text{eV}$, where the system hosts a localized MBS and an ABS, respectively. In both cases the density of states is significant only near the ends of the wire. (c),(d) Spin-resolved currents correlation $P_{\uparrow\downarrow}$ vs V at different temperatures for (c) the MBS and (d) the ABS. For the Majorana case, $P_{\uparrow\downarrow}$ is negative and goes to zero at large V . This is in striking contrast to the case of an ABS (c), where $P_{\uparrow\downarrow}$ is positive and approaches a finite constant value at large V .

The spin-resolved current correlation $P_{\uparrow\downarrow}$, on the other hand, is qualitatively different for the two cases. Figure 2(c) and Fig. 2(d) show $P_{\uparrow\downarrow}$ as a function of bias for the MBS ($B = 350 \mu\text{eV}$) and for the ABS ($B = 90 \mu\text{eV}$), respectively. As anticipated, in the case of a MBS the correlations are negative and approach zero at high voltages. In the case of an ABS, the correlations are positive and approach a finite value at large V . This is in agreement with the analytical low-energy treatment which resulted in Eq. (6) and Eq. (11).

Interestingly, the main features distinguishing a MBS from an ABS survive even at finite temperatures, as apparent in Figs. 2(c) and 2(d). At a finite temperature, $P_{\uparrow\downarrow} \neq 0$ at zero voltage. $P_{\uparrow\downarrow}$ recovers its low- T behavior at voltage $V \gtrsim T$. In particular, one can witness these distinctive features even for $T > \Gamma$. We note that

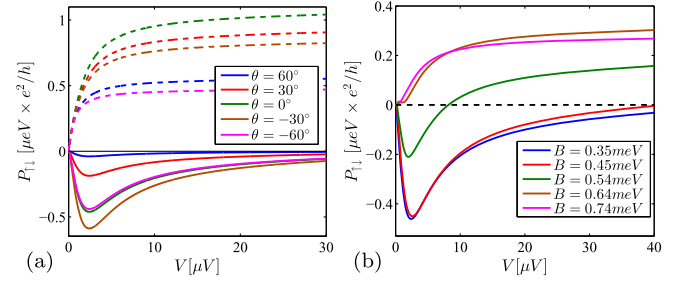


FIG. 3 (color online). Spin-resolved current correlations $P_{\uparrow\downarrow}$ as a function of bias voltage V , at $T = 0$. (a) The spin-resolved currents are defined with respect to an axis which is rotated by an angle θ from the z axis in the xz plane. The direction of \mathbf{B} remains fixed at an angle of 60° from the z axis. The characteristic features seem to be angle independent for both the Majorana bound state (MBS) $B = 350 \mu\text{eV}$ (solid lines), and the trivial Andreev bound state (ABS), $B = 90 \mu\text{eV}$ (dashed lines). (b) Crossover between a MBS and an ABS. As B is increased the spatial overlap of the pair of Majorana end states increases until they are indistinguishable from an ordinary ABS [cf. marked points in Fig. 2(a)].

Figs. 2(c) and 2(d) present results for voltages that are smaller than the excitation gap in the system (roughly $50 \mu\text{eV}$). At higher voltages the features of $P_{\uparrow\downarrow}$ are no longer universal as $P_{\uparrow\downarrow}$ picks up contributions from higher-energy resonances [45].

The spin-resolved currents whose correlation is presented in Figs. 2(c) and 2(d) are all defined with respect to the z spin axis. In Fig. 3(a) we present $P_{\uparrow\downarrow}$ for spin-resolved currents defined with a spin axis rotated by an angle θ from the z axis in the xz plane [45]. The results for the MBS (solid lines) and for the ABS (dashed lines) are obtained at zero temperature and for the same parameters as those of Fig. 2(c) and Fig. 2(d), respectively. It is apparent that the same distinctive features persist upon rotating the spin axis. We point out the suppression of $P_{\uparrow\downarrow}$ in the MBS case for $\theta = 60^\circ$, which is the direction of \mathbf{B} . This is caused due to polarization of the Majorana wave function [50,51] in the \mathbf{B} direction, giving rise to a nearly perfect polarization of the spin-resolved current through the MBS.

It is interesting to examine the crossover between the MBS case and the ABS case. This can be done by increasing B to the point where there is a large overlap between the MBSs at the two ends of the wire. At this point, the two Majorana states are equivalent to a single ordinary ABS. In particular, they are both coupled to the lead with comparable strengths. In Fig. 3(b) we present $P_{\uparrow\downarrow}$ vs V for various Zeeman energies B , corresponding to two MBSs with increasing spatial overlap. As the overlap increases, $P_{\uparrow\downarrow}$ turns from being negative to being positive for all V . We note that for all these values of B a ZBCP is present in the differential conductance spectra [cf. Fig. 2(a)].

Discussion.—We have shown that a MBS has unique signatures in spin-resolved current correlations, distinguishing

it from a topologically trivial ABS. These signatures are rooted in the nonlocal nature of the MBS. We expect other low-energy resonances, such as a Kondo resonance [52–54], or end modes due to smooth confinement in a nontopological state [27], to behave qualitatively like an ABS.

Finally, we discuss the proposed realization of the spin filters described in Fig. 1. Gates located underneath each of the two normal legs of the junction define two quantum dots. By varying the gate potential under the dot, one can tune a level of a certain spin to be at resonance, thereby filtering the spin-resolved current through that leg [55]. If the two dots are tuned to opposite spin resonances, $P_{\uparrow\downarrow}$ can be obtained by measuring correlations between the currents through the two normal legs. Alternatively, spin filters can be constructed by coupling the normal legs to oppositely polarized ferromagnets [43] or to a quantum spin Hall insulator [56–59].

We would like to acknowledge C. W. J. Beenakker, A. Yacoby, M. Heiblum, B. I. Halperin, L. Fu, J. D. Sau, P. W. Brouwer, F. Pientka, I. C. Fulga, Y. Schattner, A. Keselman, E. Sagi, D. Mark, and K. Kaasbjerg. This study was supported by the Israel Science Foundation (ISF), a Career Integration Grant (CIG), the German-Israeli Foundation (GIF), the Minerva Foundation, the Helmholtz Virtual Institute—“New States of Matter and their Excitations,” and an ERC grant (FP7/2007-2013) 340210.

-
- [1] J. Alicea, *Rep. Prog. Phys.* **75**, 076501 (2012).
 [2] C. W. J. Beenakker, *Annu. Rev. Condens. Matter Phys.* **4**, 113 (2013).
 [3] A. Y. Kitaev, *Phys. Usp.* **44**, 131 (2001).
 [4] D. A. Ivanov, *Phys. Rev. Lett.* **86**, 268 (2001).
 [5] A. Stern, F. von Oppen, and E. Mariani, *Phys. Rev. B* **70**, 205338 (2004).
 [6] C. Nayak, S. Simon, A. Stern, M. Freedman, and S. Sarma, *Rev. Mod. Phys.* **80**, 1083 (2008).
 [7] J. Alicea, Y. Oreg, G. Refael, F. von Oppen, and M. P. Fisher, *Nat. Phys.* **7**, 412 (2011).
 [8] A. Y. Kitaev, *Ann. Phys. (Amsterdam)* **303**, 2 (2003).
 [9] N. Read and D. Green, *Phys. Rev. B* **61**, 10267 (2000).
 [10] G. Moore and N. Read, *Nucl. Phys.* **B360**, 362 (1991).
 [11] L. Fu and C. L. Kane, *Phys. Rev. Lett.* **100**, 096407 (2008).
 [12] L. Fu and C. L. Kane, *Phys. Rev. B* **79**, 161408 (2009).
 [13] J. D. Sau, R. M. Lutchyn, S. Tewari, and S. Das Sarma, *Phys. Rev. Lett.* **104**, 040502 (2010).
 [14] J. Alicea, *Phys. Rev. B* **81**, 125318 (2010).
 [15] R. M. Lutchyn, J. D. Sau, and S. Das Sarma, *Phys. Rev. Lett.* **105**, 077001 (2010).
 [16] Y. Oreg, G. Refael, and F. von Oppen, *Phys. Rev. Lett.* **105**, 177002 (2010).
 [17] V. Mourik, K. Zuo, S. Frolov, S. Plissard, E. Bakkers, and L. Kouwenhoven, *Science* **336**, 1003 (2012).
 [18] M. T. Deng, C. L. Yu, G. Y. Huang, M. Larsson, P. Caroff, and H. Q. Xu, *Nano Lett.* **12**, 6414 (2012).
 [19] A. Das, Y. Ronen, Y. Most, Y. Oreg, M. Heiblum, and H. Shtrikman, *Nat. Phys.* **8**, 887 (2012).
 [20] H. O. H. Churchill, V. Fatemi, K. Grove-Rasmussen, M. T. Deng, P. Caroff, H. Q. Xu, and C. M. Marcus, *Phys. Rev. B* **87**, 241401 (2013).
 [21] A. D. K. Finck, D. J. Van Harlingen, P. K. Mohseni, K. Jung, and X. Li, *Phys. Rev. Lett.* **110**, 126406 (2013).
 [22] K. T. Law, P. A. Lee, and T. K. Ng, *Phys. Rev. Lett.* **103**, 237001 (2009).
 [23] C. J. Bolech and E. Demler, *Phys. Rev. Lett.* **98**, 237002 (2007).
 [24] L. Fidkowski, J. Alicea, N. H. Lindner, R. M. Lutchyn, and M. P. A. Fisher, *Phys. Rev. B* **85**, 245121 (2012).
 [25] S. Nadj-Perge, I. K. Drozdov, J. Li, H. Chen, S. Jeon, J. Seo, A. H. MacDonald, B. A. Bernevig, and A. Yazdani, *Science* **346**, 602 (2014).
 [26] D. I. Pikulin, J. P. Dahlhaus, M. Wimmer, H. Schomerus, and C. W. J. Beenakker, *New J. Phys.* **14**, 125011 (2012).
 [27] G. Kells, D. Meidan, and P. W. Brouwer, *Phys. Rev. B* **86**, 100503 (2012).
 [28] J. Liu, A. C. Potter, K. T. Law, and P. A. Lee, *Phys. Rev. Lett.* **109**, 267002 (2012).
 [29] S. Sasaki, S. De Franceschi, J. Elzerman, W. Van der Wiel, M. Eto, S. Tarucha, and L. Kouwenhoven, *Nature (London)* **405**, 764 (2000).
 [30] D. Bagrets and A. Altland, *Phys. Rev. Lett.* **109**, 227005 (2012).
 [31] E. J. Lee, X. Jiang, M. Houzet, R. Aguado, C. M. Lieber, and S. De Franceschi, *Nat. Nanotechnol.* **9**, 79 (2014).
 [32] A. F. Andreev, *Zh. Eksp. Teor. Fiz.* **46**, 1823 (1964) [*Sov. Phys.-JETP* **19**, 1228 (1964)].
 [33] Note that this process can happen more than once since charge is not conserved in the superconductor.
 [34] Formally this reads $\langle 0 | s(x) | 0 \rangle = \langle 1 | s(x) | 1 \rangle$, where $s(x)$ is the spin density and $|0\rangle, |1\rangle$ are the two degenerate ground states.
 [35] Although we consider here a single-channel lead, our conclusions extend to a multichannel lead.
 [36] D. S. Fisher and P. A. Lee, *Phys. Rev. B* **23**, 6851 (1981).
 [37] S. Iida, H. Weidenmüller, and J. Zuk, *Ann. Phys. (N.Y.)* **200**, 219 (1990).
 [38] M. P. Anantram and S. Datta, *Phys. Rev. B* **53**, 16390 (1996).
 [39] A. Golub and B. Horovitz, *Phys. Rev. B* **83**, 153415 (2011).
 [40] A. Golub and B. Horovitz, *arXiv:1407.5179*.
 [41] J. Nilsson, A. R. Akhmerov, and C. W. J. Beenakker, *Phys. Rev. Lett.* **101**, 120403 (2008).
 [42] M. Leijnse and K. Flensberg, *Phys. Rev. Lett.* **107**, 210502 (2011).
 [43] J. J. He, T. K. Ng, P. A. Lee, and K. T. Law, *Phys. Rev. Lett.* **112**, 037001 (2014).
 [44] We shall show using numerical simulations of a system with spin-orbit coupling that our conclusions apply also for an ABS with a non-well-defined spin.
 [45] See Supplemental Material at <http://link.aps.org/supplemental/10.1103/PhysRevLett.114.166406> for more details on the numerical simulations, the ABS model, rotations in spin space and additional results.
 [46] J. S. Lim, L. Serra, R. López, and R. Aguado, *Phys. Rev. B* **86**, 121103 (2012).

- [47] S. Das Sarma, J. D. Sau, and T. D. Stanescu, *Phys. Rev. B* **86**, 220506 (2012).
- [48] D. Rainis, L. Trifunovic, J. Klinovaja, and D. Loss, *Phys. Rev. B* **87**, 024515 (2013).
- [49] Note that the wave function has support in the uncovered part of the wire, see J. Klinovaja and D. Loss, *Phys. Rev. B* **86**, 085408 (2012).
- [50] D. Sticlet, C. Bena, and P. Simon, *Phys. Rev. Lett.* **108**, 096802 (2012).
- [51] M. Guigou, N. Sedlmayr, J. Aguiar-Hualde, and C. Bena, [arXiv:1407.1393](https://arxiv.org/abs/1407.1393).
- [52] J. C. Cuevas, A. Levy Yeyati, and A. Martín-Rodero, *Phys. Rev. B* **63**, 094515 (2001).
- [53] E. J. H. Lee, X. Jiang, R. Aguado, G. Katsaros, C. M. Lieber, and S. De Franceschi, *Phys. Rev. Lett.* **109**, 186802 (2012).
- [54] M. Cheng, M. Becker, B. Bauer, and R. M. Lutchyn, *Phys. Rev. X* **4**, 031051 (2014).
- [55] The width of the resonance has to be comparable with the voltage range of interest. Since B is commonly larger than the excitation gap, this can be achieved without allowing transmission of opposite spins.
- [56] T. Posske and B. Trauzettel, *Phys. Rev. B* **89**, 075108 (2014).
- [57] C. L. Kane and E. J. Mele, *Phys. Rev. Lett.* **95**, 226801 (2005).
- [58] B. A. Bernevig, T. L. Hughes, and S.-C. Zhang, *Science* **314**, 1757 (2006).
- [59] M. König, S. Wiedmann, C. Brüne, A. Roth, H. Buhmann, L. W. Molenkamp, X.-L. Qi, and S.-C. Zhang, *Science* **318**, 766 (2007).